JACS
JOURNAL OF THE AMERICAN CHEMICAL SOCIETY
Article
pubs.acs.org/JACS

Importance of Metal Hydration on the Selectivity of Mg^{2+} versus Ca^{2+} in Magnesium Ion Channels

Todor Dudev*[,†,§] and Carmay Lim*[,†,‡]

[†]Institute of Biomedical Sciences, Academia Sinica, Taipei 11529, Taiwan
[‡]Department of Chemistry, National Tsing Hua University, Hsinchu 300, Taiwan

ABSTRACT: Magnesium ion channels and transporters regulate the cellular concentrations of Mg^{2+}, which must be tightly controlled as imbalances have been associated with diseases such as osteoporosis, diabetes, and high blood pressure in humans. The channels and transporters allow the "native" Mg^{2+} to be transported against a high background concentration of its major competitor, Ca^{2+}. Their selectivity filters (the narrowest part of the open pore) control metal ion selectivity. As the structures of Mg^{2+} channels in an open conformation with bound Mg^{2+} have not yet been solved, the key determinants of Mg^{2+}/Ca^{2+} selectivity in Mg^{2+} ion channels remain elusive. Here, using density functional theory combined with continuum dielectric methods, we evaluated how the competition between Mg^{2+} and Ca^{2+} in model selectivity filters depends on the degree of metal hydration, which correlates with the pore size/rigidity as well as the composition and solvent accessibility of the selectivity filter. The key determinant of the selectivity for Mg^{2+} over Ca^{2+} in the Mg^{2+} channel selectivity filter is a pore that is sufficiently large to accommodate hexahydrated Mg ions. In such wide pores, the hexahydrated metal ions interact indirectly with the protein ligands, hence metal desolvation and ligand−ligand steric repulsion become less important than Mg^{2+}−water−protein interactions. These wide pores are Mg^{2+}-selective because compared to Ca^{2+} or Na^{+} and K^{+} monocations, Mg^{2+} better polarizes the bound water molecules resulting in stronger Mg^{2+}−water−protein interactions. Although both tetrameric and pentameric filters with pores that can accommodate hexahydrated metal ions could select Mg^{2+} over Ca^{2+}, a bilayered pentameric filter lined with a ring of amides and a ring of carboxylates seems to best discriminate the "native" Mg^{2+} from its key rival, Ca^{2+}. Our results are consistent with available experimental data and help to elucidate the selectivity filters in the Mg^{2+}-selective TRPM6 and CorA channels.

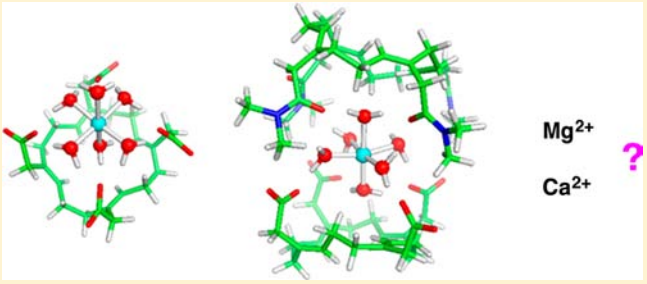

INTRODUCTION

Magnesium is one of the most abundant divalent metal cations in both prokaryotic and eukaryotic cells. Its total cellular concentration is 15−25 mM with a free concentration of 0.3−1.5 mM.[1−5] It is an indispensable element for life and one of the most versatile metal cofactors in biochemistry, serving both intra- and extracellular roles.[6] It can play a catalytic role, serving as an essential cofactor in many enzymes involved in regulating nucleic acid biochemistry and protein synthesis or an exclusively structural role, stabilizing various protein structures, nucleic acids, and biological membranes. In prokaryotes, Mg^{2+} is an external signaling entity controlling the organism's virulence,[7] while in green plants, Mg^{2+} is a key building block of chlorophyll.

For proper functioning, the cellular machinery has exploited several specific physicochemical properties of Mg^{2+}, which collectively render Mg^{2+} unique among the biological cations: These properties of Mg^{2+} are its small size, high mobility, high charge density, strong Lewis acidity, high binding affinity toward water and other oxygen-containing ligands (e.g., carboxylate and phosphate groups), stable coordination number (almost invariably 6), rigid octahedral ligation sphere, and relatively slow exchange rate of the Mg^{2+}-bound water molecules. Because Mg^{2+} has a large hydration free energy (~456 kcal/mol), it forms stable hydrates. In nucleic acids, Mg^{2+} retains its hydration shell and binds indirectly via water molecule(s) to the host ligands (outer-shell mode).[6] In proteins, Mg^{2+} usually binds directly to the amino acid residues lining the binding pocket (inner-shell mode), but it does not exchange all of its first-shell water molecules for protein ligands.[8,9] Consequently, Mg^{2+} often acts as a water-carrier for enzymatic reactions that require a water molecule in the active site. It polarizes or ionizes the metal-bound water and is thought to orient a catalytic water molecule for subsequent catalytic action in many Mg^{2+}-dependent enzymes.

Magnesium homeostasis in living cells is tightly controlled. Irregularities in the cytosolic Mg^{2+} concentrations adversely affect biological processes and disrupt normal functioning of the organism; in humans, this is associated with diseases such as osteoporosis, diabetes, and high blood pressure.[10] Magnesium ion channels and transporters regulate Mg^{2+} homeostasis. Several classes of Mg^{2+} ion channels in both prokaryotic and eukaryotic kingdoms have been identified. The most studied

Received: August 24, 2013
Published: October 2, 2013

   dx.doi.org/10.1021/ja4087769 | J. Am. Chem. Soc. 2013, 135, 17200−17208

are the bacterial CorA and its eukaryotic homologues ALR1/ALR2 and Mrs2, prokaryotic MgtE, and eukaryotic TRPM6 and TRPM7, which are members of the Transient Receptor Potential Melastatin subfamily.[11,12] Although these influx channels possess different structures, they can very efficiently discriminate Mg^{2+} from other metal species and allow the "native" Mg^{2+} to be transported against a high background concentration of its major competitor, Ca^{2+}: CorA, Mrs2, and MgtE are highly permeable for Mg^{2+} but do not transport Ca^{2+},[4,11] while TRPM6 has a 5-fold higher affinity for Mg^{2+} than for Ca^{2+}.[13] The metal ion selectivity of these Mg^{2+} ion channels is controlled by the selectivity filter—the narrowest part of the open pore.

To date, knowledge about the selectivity filters of Mg^{2+} channels are limited, so the key determinants of Mg^{2+}/Ca^{2+} selectivity in Mg^{2+} ion channels remain elusive. Although the atomic-resolution structure of the TRPM6 channel selectivity filter has not yet been solved, site-directed mutagenesis and electro-physiological measurements have identified a potential selectivity filter with I1030 and D1031 located at the narrowest area of the channel pore.[14] D1031 appears to be more important than I1030 in metal ion selectivity, as it is absolutely conserved among the eight members of the TRPM subfamily (TRPM1 to TRPM8) and its mutation to alanine results in a nonfunctional channel.[14] The neighboring I1030 seems to play a more modest role in the selectivity process, as its mutation to methionine results in a functional channel, but with a reduced pore diameter.[14] Notably, the experiments revealed a large TRPM6 channel pore of 11.5 Å in diameter.[14] However, there are no in-depth studies on why the TRPM6 channel is Mg^{2+}-selective.

Whereas the TRPM6 channel is a homotetramer,[13] CorA is a homopentamer with two transmembrane helices connected by a short periplasmic loop per monomer, as shown in the crystal structures of the CorA channels: The closed-state conformations of full-length *Thermotoga maritima* CorA (*Tm*CorA) have been solved at a resolution of 3.9 Å (PDB code 2bbj[15]), 3.7 Å (PDB code 2hn2[16]), and 2.7 Å (PDB code 4i0u[17]), while that of *Methanocaldococcus jannaschii* CorA (*Mj*CorA) has been solved at a resolution of 3.2 Å (PDB code 4ev6[18]). Despite the availability of several CorA structures, there is no unified view about the location/composition of the channel's selectivity filter and its interactions with the cognate cation: In *Salmonella typhimurium* CorA (*St*CorA), no crystal structure has yet been solved, but mutations of residues comprising the periplasmic loop, EF**MPEL**KWS, indicate that this loop functions as the selectivity filter through interactions with a hexahydrated cation rather than the cation itself. The glutamate in the conserved "**MPEL**" motif of this loop[12,19] has been shown to be critical for the channel's function/selectivity.[20] Instead of the **MPEL** motif, the crystal structures of *Mj*CorA[18] and *Tm*CorA[17] show that the highly conserved "**GMN**" motif at the N-terminus of the periplasmic loop serves as the selectivity filter. Although metal-bound water molecules were not seen in these two structures, the ∼4 Å distance between Mg^{2+} and the carbonyl oxygen suggests a hexahydrated cation in a relatively large selectivity filter pore with a diameter of ∼8 Å. Interestingly, the Mg^{2+} indirectly coordinates each Asn from the GMN motif in the 3.2-Å structure of *Mj*CorA (PDB code 4ev6[18]), but each Gly from the same motif in the 2.7-Å structure of *Tm*CorA (PDB code 4i0u[17]). Hence, it remains unclear whether the CorA selectivity filter is composed of carbonyl oxygen atoms from the GMN motif or carboxylate oxygen atoms from the MPEL motif and how such a filter can distinguish hexahydrated Mg^{2+} among similarly hydrated divalent ions.

Herein, we endeavor to unravel the basic determinants of Mg^{2+}/Ca^{2+} selectivity in Mg^{2+} ion channel selectivity filters by addressing the following questions:

1. How strongly is the metal ion competition affected by changes in the pore size/rigidity, solvent accessibility, and composition of the Mg^{2+} channel selectivity filter?
2. To what extent does the degree of metal hydration affect the metal ion competition in Mg^{2+} channel selectivity filter?
3. Which type of selectivity filter best discriminates the "native" Mg^{2+} from its key rival, Ca^{2+}?
4. What are the major determinants of metal ion selectivity in Mg^{2+} channels and how do they compare with those in other types of cation channels?

To address these questions, we modeled various selectivity filters, differing in size, oligomericity, composition, and number of layers (see Methods) and evaluated their metal selectivity properties. The metal ions and first-shell ligands, which play a key role in the Mg^{2+}/Ca^{2+} competition, were treated explicitly using density functional theory, while the region inside the selectivity filter was represented by an effective dielectric constant varying from 4 to 30, mimicking binding sites of increased solvent exposure. The aim of the calculations is to yield reliable trends in the free energy changes with varying parameters such as the size of the pore, rather than to reproduce the absolute metal exchange free energies in the selectivity filters. Notably, the methodology employed herein has yielded trends in the free energy changes in previous works that are in line with experimental observations.[21−28]

METHODS

Selectivity Filter Models and Justification. Since mutagenesis and crystallographic studies, respectively, indicate homotetrameric and homopentameric selectivity filters in Mg^{2+} channels lined with Asp/Glu or Asn side chains and/or backbone peptide groups, selectivity filters containing four or five metal-ligating groups such as $-COO^-$ (representing Asp/Glu side chains) and $-CONH_2$ (representing the Asn side chain or backbone peptide group) were modeled (see Figures 1 and 2). Furthermore, since it is unclear if one or two layers of metal-ligating residues lining the selectivity filter select the "right" cation in the Mg^{2+} channel, both monolayered (Figures 3a,b and 4a,b) and bilayered (Figures 3c and 4c) selectivity filters were constructed. The $-CONH_2$ groups in the monolayered filters were methylated to $-CON(CH_3)_2$ in the bilayer structures to avoid interlayer COO...NH hydrogen bond formation and disruption of the overall structure. The metal-ligating groups were coordinated to the permeating ion (Ca^{2+} or Mg^{2+}) and attached to a carbon−hydrogen ring scaffold via methylene spacers (Figures 1−4). Models of the tetrameric and pentameric selectivity filters were built using GaussView version 3.09,[29] following the guidelines from our previous work.[26] They were designed to maximize resemblance to the selectivity filters of Mg^{2+} channels and were constructed on the basis of the following considerations: (a) The ring mimics the oligomeric state of the ion channel pore. (b) The ring scaffold mimics the role of the second metal coordination shell in properly orienting the metal-ligating groups so that they can interact with the passing cation without obstructing the permeation pathway. Detaching the ligands from the ring scaffold would lead to unrealistic structures where the pore-like shape is lost with one or two ligating groups occluding the ion passage pathway, as shown in our previous work.[30] (c) The metal-ligating groups and their connection to the ring are flexible enough to allow them to optimize their positions upon metal binding. The shape and C−H orientations of the ring do not obstruct the pore lumen and impede the metal-ligating groups from

dx.doi.org/10.1021/ja4087769 | J. Am. Chem. Soc. 2013, 135, 17200−17208

Table 1. Comparison between Computed and Experimental Free Energies of Metal Exchange, ΔG_{ex}^{80}, in Crown Ether and Nitrilotriacetic Acid (NTA) Complexes

reaction	ΔG^{80} (kcal/mol)		
	expt	calcd	error[a]
$[Na(H_2O)_6]^+ + [K\ (18\text{-crown-}6)]^+ \rightarrow [K(H_2O)_6]^+ + [Na(18\text{-crown-}6)]^+$	2.0[b]	1.4[c]	−0.6
$[Na(H_2O)_6]^+ + [Ca(H_2O)_2(NTA)]^- + H_2O \rightarrow [Ca(H_2O)_7]^{2+} + [Na(H_2O)_2(NTA)]^{2-}$	7.1[d]	6.7[e]	−0.4
$[Mg(H_2O)_6]^{2+} + [Ca(H_2O)_2(NTA)]^- + H_2O \rightarrow [Ca(H_2O)_7]^{2+} + [Mg(H_2O)_2(NTA)]^-$	1.2[d]	0.4[e]	−0.8

[a]Error = ΔG^{80}(calcd) − ΔG^{80}(expt). [b]From Ozutsumi and Ishigiro, 1992.[42] [c]From Dudev and Lim.[41] [d]Calculated from the experimental stability constants of the respective metal complexes from Smith and Martell, 1987.[43] [e]From Dudev and Lim.[30]

coordinating to the metal.[26] (d) The ring's chain length would not bias the results, as the number of carbon atoms in the tetrameric ring (16) is similar to that in its pentameric counterpart (15).

Reaction Modeled. The outcome of the competition between the bulk solvent and the protein ligands for the native cation in an ion selectivity filter was assessed by computing the free energy for replacing Ca^{2+} bound inside the model selectivity filter, $[Ca(H_2O)_n$-filter], with Mg^{2+}:

$$[Mg(H_2O)_6]^{2+} + [Ca(H_2O)_n\text{-filter}] + H_2O \rightarrow [Mg(H_2O)_n\text{-filter}] + [Ca(H_2O)_7]^{2+} \quad (1)$$

where n = 0, 1, 2, or 6. In eq 1, $[Mg(H_2O)_6]^{2+}$ and $[Ca(H_2O)_7]^{2+}$ aqua complexes were modeled, as the hydration numbers of six and seven are the most common in Mg^{2+} and Ca^{2+} hydrates, respectively.[31,32] The ion exchange free energy for eq 1 in an environment characterized by an effective dielectric constant x is given by,

$$\Delta G^x = \Delta G^1 + \Delta G_{solv}{}^x([Mg(H_2O)_n\text{-filter}]) + \Delta G_{solv}{}^x([Ca(H_2O)_7]) - \Delta G_{solv}{}^x([Ca(H_2O)_n\text{-filter}]) - \Delta G_{solv}{}^x([Mg(H_2O)_6]) - \Delta G_{solv}{}^x(H_2O) \quad (2)$$

where ΔG^1 is the gas-phase free energy for eq 1 and $\Delta G_{solv}{}^x$ is the free energy for transferring a molecule in the gas phase to a medium characterized by an effective dielectric constant x. A positive ΔG^x implies a Ca^{2+}-selective filter, whereas a negative value implies a Mg^{2+}-selective one.

Gas-Phase Free Energy Calculations. Among several combinations of different ab initio/density functional theory methods (HF, MP2, S-VWN and B3-LYP) and basis sets (6-31+G(d,p), 6-31+G(2d,2p), 6-31+G(3d,p), 6-31+G(3d,2p), 6-311++G(d,p) and 6-311++G(3df,3pd)), the B3-LYP/6-31+G(3d,p) method had been shown to be the most efficient in yielding dipole moments of the metal ligands that are closest to the respective experimental values; it can also reproduce (within experimental error) the metal−oxygen bond distances in aqua and crown-ether complexes, which resemble metal-occupied ion channel pores.[26] Hence, the B3-LYP/6-31+G(3d,p) method was used to optimize the geometry of each metal complex without any constraints and to compute the electronic energies, E_{el}, using the Gaussian 09 program.[33] Frequency calculations for each optimized monolayered structure were performed at the same level of theory; these calculations required roughly one week on six dual Intel XEON CPUs. No imaginary frequency was found for any of the optimized structures. The B3-LYP/6-31+G(3d,p) frequencies were scaled by an empirical factor of 0.9613[34] and used to compute the thermal energies including zero-point energy (E_{th}) and entropies (S). The differences ΔE_{el}, ΔE_{th}, ΔPV (work term), and ΔS between the products and reactants in eq 1 were used to calculate the gas-phase ΔG^1 free energy at T = 298.15 K according to

$$\Delta G^1 = \Delta E_{el} + \Delta E_{th} + \Delta PV - T\Delta S \quad (3)$$

For the two-layered Mg^{2+} and Ca^{2+} complexes (Figures 3c and 4c), geometry optimization took several months on six dual Intel XEON CPUs. Frequency calculations were computationally prohibitive due to the large number of basis functions (between 2913 and 3165) used to optimize these structures. Hence, the corresponding thermal energies and entropies for these complexes could not be evaluated, so E_{th} and S for the metal-occupied two-layered selectivity filters were not included in calculating the respective ΔG^1. However, for the type of ion exchange reactions described by eq 1, our previous calculations[26] showed that neglecting these ΔE_{th} and $T\Delta S$ terms in evaluating the free energies of metal exchange in large model selectivity filters alters ΔG^1 by less than 1 kcal/mol. They also showed the basis set superposition error to be negligible, which was thus not considered in the present calculations.

Solution Free Energy Calculations. The $\Delta G_{solv}{}^x$ (x = 4, 10, or 30) values were estimated by solving Poisson's equation using finite difference methods[35,36] with the MEAD (macroscopic electrostatics with atomic detail) program,[37] as described in previous works.[38] Natural Bond Orbital atomic charges, which are known to be numerically quite stable with respect to basis set changes,[39] were employed in the calculations. The effective solute radii were obtained by adjusting the CHARMM (version 22)[40] van der Waals radii to reproduce the experimental hydration-free energies of Mg^{2+}, Ca^{2+}, and model ligand molecules to within 1 kcal/mol.[28,30] The resulting values (in Å) are as follows: R_{Mg} = 1.50, R_{Ca} = 1.75, R_C = 1.95, R_N = 1.75, $R_O(-COO)$ = 1.56, $R_O(-CONH_2/CON(CH_3)_2)$ = 1.72, $R_O(H_2O)$ = 1.85, $R_O(Mg/Ca-H_2O)$ = 1.84, $R_O(Mg-COO)$ = 1.34, $R_O(Ca-COO)$ = 1.25, R_H = 1.50, $R_H(H_2O-Mg)$ = 1.125, $R_H(H_2O-Ca)$ = 1.053.

Validation of Models/Methodology. The above methodology had been validated against experimental ion exchange free energies between biogenic metal cations such as Na^+, K^+, Mg^{2+}, and Ca^{2+} in systems resembling either the selectivity filter pores (crown ethers; Table 1)[41] or in systems containing carboxylic ligands (nitrilotriacetic acid; Table 1)[30] with interactions that are similar to the Asp/Glu carboxylates lining the selectivity filters of ion channels. As shown in Table 1, the computed metal exchange free energies are in line with the experimental estimates to within 1 kcal/mol.

The approach used herein had also yielded trends in metal exchange free energies in model selectivity filters in accord with the experimentally observed metal selectivity: Both theory and experiment show that the DEKA selectivity filter in the wild-type voltage-gated Na^+ (Na_v) channels are highly selective for Na^+/K^+, whereas mutant DERA and DEEA filters exhibit decreased and reversed Na^+/K^+ selectivity, respectively.[27] They also show that the narrow EEEE selectivity filters found in voltage-gated Ca^{2+} (Ca_v) channels that fit monohydrated ions are Ca^{2+}/Na^+-selective, whereas larger EEEE pores found in Na_v channels that fit dihydrated ions in the plane of the selectivity ring are Na^+/Ca^{2+}-selective (see Discussion section).[30] Notably, the computed pore aperture areas for several model selectivity filters overlap with the experimental estimates: The computed pore areas for the model EEEE selectivity filters in Ca_v channels (15−19 Å^2) and in bacterial Na_v channels (20−25 Å^2) agree with the experimental estimates of 18−19 Å^2 and ∼21 Å^2, respectively.[44] Furthermore, our previous calculations showed that distal interactions in the channel protein, which were not explicitly considered in the present calculations, contribute very little to the metal-exchange energy in the EEEE filter and would not be expected to affect the results obtained.[30]

III. RESULTS

Narrow Pores That Bind Dehydrated Ions are Ca^{2+}-Selective. Both mutagenesis and crystallographic studies

indicate that Mg^{2+} channels have pores that are too large for a fully dehydrated Mg^{2+} ion to bind directly to Asp/Asn or backbone peptide groups lining the selectivity filter. To test the hypothesis that Mg^{2+} channels do not recognize dehydrated metal cations, we computed the free energies for replacing Ca^{2+} bound directly to ligands in tetrameric and pentameric filters with dehydrated Mg^{2+}. Figure 1 shows the optimized structures

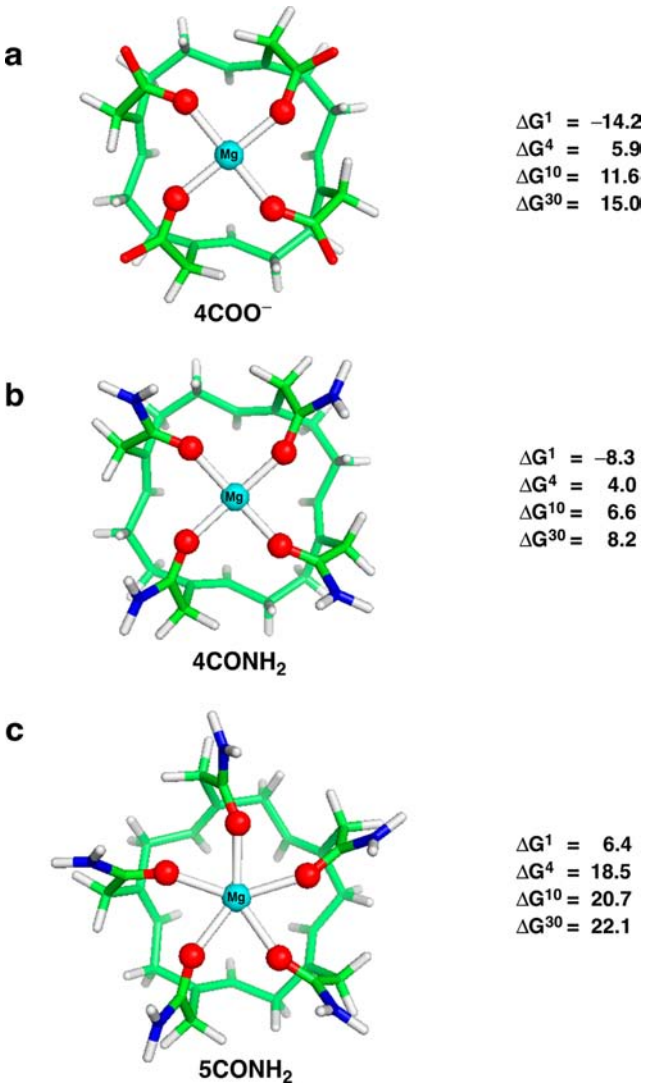

Figure 1. B3-LYP/6-31+G(3d,p) optimized structures of Mg^{2+}-bound model selectivity filters comprising (a) four COO^- groups (representing Asp/Glu side chains), (b) four $CONH_2$ groups (representing Asn/Gln side chains or backbone peptide groups), and (c) five $CONH_2$ groups. The free energies ΔG^x (in kcal/mol) for replacing Ca^{2+} in the filter characterized by dielectric constant x with Mg^{2+} (eq 1) are shown on the right.

of the Mg^{2+}-bound model selectivity filters and the $Ca^{2+} \rightarrow Mg^{2+}$ exchange free energies, ΔG^x, for pores characterized by an effective dielectric constant x ranging from 4 to 30. The positive ΔG^x (x = 4−30) values in Figure 1 confirm the hypothesis that tetrameric and pentameric Mg^{2+} channels with narrow pores that fit dehydrated as opposed to hydrated metal ions cannot select Mg^{2+}, but favor Ca^{2+} instead. The preference for Ca^{2+} over Mg^{2+} in such narrow pores is largely because the cost of removing first-shell water molecules from Mg^{2+} is greater than that from Ca^{2+}. This cost outweighs the gain in electrostatic interactions with the amide or carboxylate groups by the better electron acceptor Mg^{2+} compared to Ca^{2+}, which is evidenced by the favorable $Ca^{2+} \rightarrow Mg^{2+}$ gas-phase free energies in the model tetrameric filters (Figure 1a,b, negative ΔG^1). Note that the gas-phase free energy is dictated by the enthalpic term, while the $T\Delta S$ contribution is much smaller (∼4−6 kcal/mol). Increasing the oligomericity of the channel also significantly enhances selectivity for Ca^{2+} over Mg^{2+} in a narrow pore: the free energies in the pentameric filter (Figure 1c) are more positive than those in the respective tetrameric filter (Figure 1b), as steric repulsion among five carbonyl oxygen atoms bound to the small Mg^{2+} is greater than that around the larger Ca^{2+}: the gas-phase ΔG^1 free energy for the tetrameric **4CONH$_2$** filter (Figure 1b), which is negative (−8.3 kcal/mol), becomes positive for the pentameric **5CONH$_2$** filter (6.4 kcal/mol, Figure 1c).

Metal Hydration Significantly Affects the Channel's Selectivity. To assess the effect of metal hydration on the competition between Mg^{2+} and Ca^{2+}, we computed the free energies for replacing Ca^{2+} with Mg^{2+} in model selectivity filters, ΔG^x (x = 4−30), with varying pore size that can accommodate metal cations with different hydration numbers. Pentameric filters lined with amide ligands with the metal cation bound to zero (**5CONH$_2$**), one (**5CONH$_2$/1W**), two (**5CONH$_2$/2W**), and six (**5CONH$_2$/6W**) water molecules were fully optimized. Their pore aperture areas were estimated by the area of the pentagon formed by connecting the five amide oxygen atoms in each optimized structure. These areas show that the pore size correlates with increasing metal hydration: the pore aperture areas are 11, 18, 25, and 32 Å^2 for the **5CONH$_2$**, **5CONH$_2$/1W**, **5CONH$_2$/2W**, and **5CONH$_2$/6W** structures, respectively.

Increasing pore size/metal hydration significantly enhances the selectivity for Mg^{2+} over Ca^{2+}: The gas-phase ΔG^1 $Ca^{2+} \rightarrow Mg^{2+}$ free energy for the **5CONH$_2$** filter, whose pore fits dehydrated metal ions, is unfavorable (6.4 kcal/mol, Figure 2a), but becomes quite favorable in a wider pore fitting monohydrated metal (−14.6 kcal/mol, Figure 2b). Note that the sign of the ΔG^1 free energy changes as the coordination number of the metal in the **5CONH$_2$** filter changes from five to four for the metal in the **5CONH$_2$/1W** (Figure 2b) or tetrameric **4CONH$_2$** filter (Figure 1b). This huge drop of ∼21 kcal/mol in the ΔG^1 upon increasing the pore in the **5CONH$_2$** filter to fit a monohydrated metal is partly because the steric repulsion among the five carbonyl oxygen atoms in the first coordination shell is relieved when two of the carbonyl oxygen atoms move to the second coordination shell and interact via a bound water with Mg^{2+}. It is also due to the stronger electron-accepting ability of Mg^{2+}, which polarizes its first-shell water molecule(s) more than Ca^{2+}, resulting in stronger metal−water−carbonyl electrostatic interactions in the Mg^{2+} complexes than in the respective Ca^{2+} clusters. The gas-phase ΔG^1 free energy further decreases to −15.5 and −17.9 kcal/mol in an increasingly wide pore fitting dihydrated (Figure 2c) and hexahydrated (Figure 2d) cations, respectively. The protein environment does not change the gas-phase free energy trends observed: The ΔG^x (x = 4−30) decreases with increasing pore size and the metal hydration number. For the series of filters shown in Figure 2, the highest selectivity for Mg^{2+} over Ca^{2+} is predicted for a pore that can accommodate a hexahydrated cation, which binds indirectly to the amide groups lining the pore (Figure 2d; **5CONH$_2$/6W**). Such a pore appears to be

dx.doi.org/10.1021/ja4087769 | J. Am. Chem. Soc. 2013, 135, 17200−17208

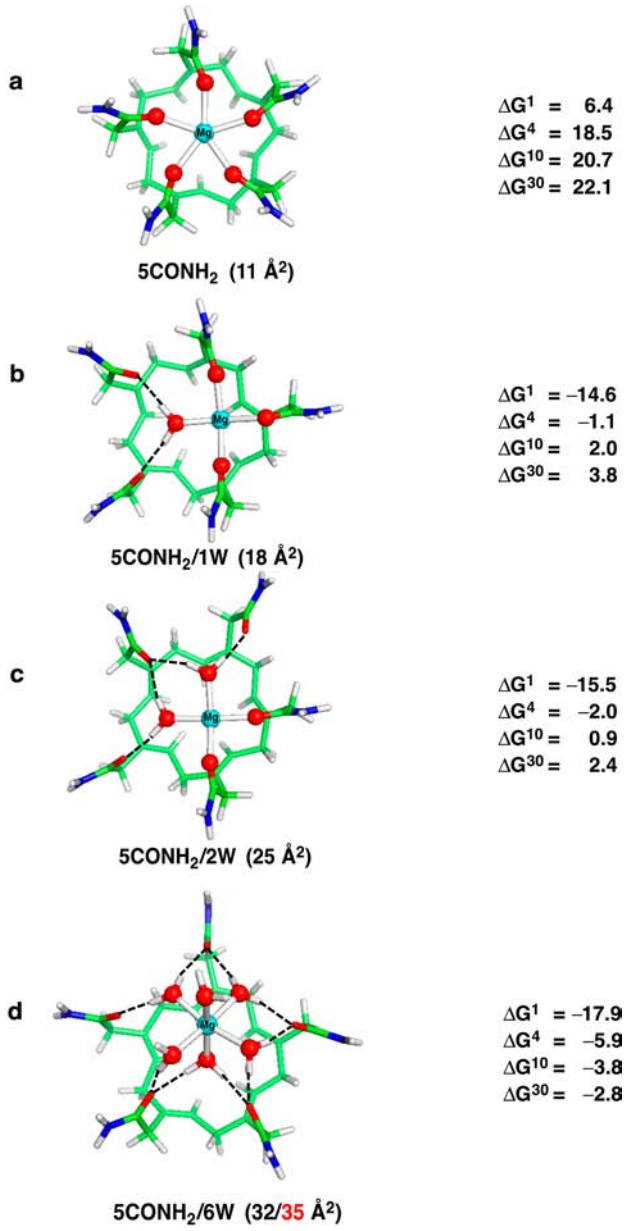

Figure 2. B3-LYP/6-31+G(3d,p) optimized structures of Mg^{2+}-bound model selectivity filters comprising five $CONH_2$ ligating groups with the metal bound to (a) 0, (b) 1, (c) 2, and (d) 6 water molecules. The free energies ΔG^x (in kcal/mol) for replacing Ca^{2+} in the filter characterized by dielectric constant x with Mg^{2+} (eq 1) are shown on the right. The aperture area of the pore, estimated by the area of the pentagon formed by the five amide oxygen atoms, is shown in parentheses. The value highlighted in red corresponds to the aperture area estimated from the experimentally observed Mg^{2+}−O(Gly312) distance of 3.97 Å in the 2.7 Å crystal structure of *Tm*CorA (PDB code 4i0u).

Mg^{2+}-selective over a wide range in the pore's effective dielectric constant (Figure 2d, negative ΔG^x for x = 4−30).

Wide Pores That Bind Hexahydrated Ions are Mg^{2+}-Selective. Since experimental data suggest that the Mg^{2+} channel binds fully hexahydrated Mg^{2+}, we computed the free energies for replacing hexahydrated Ca^{2+} with hexahydrated Mg^{2+} in model tetrameric (Figure 3) and pentameric filters (Figure 4), representing the selectivity filters of the Mg^{2+}-selective TRPM6 and CorA ion channels, respectively.

Tetrameric Filters. The selectivity filter of the homotetrameric TRPM6 ion channel has an estimated pore diameter of ∼11.5 Å, comprising I1030 and D1031 residues (see Introduction).[14] However, it is not clear whether the metal binds to a monolayer of I1030 carbonyl oxygen or D1031 carboxylate oxygen atoms or to a bilayer of both I1030 carbonyl oxygen and D1031 carboxylate oxygen atoms. Hence, we modeled tetrameric selectivity filters lined with (a) a single layer of amide ligands modeling the Ile backbone amide (Figure 3a, **4CONH$_2$/6W**), (b) a single layer of carboxylates modeling the Asp/Glu side chains (Figure 3b, **4COO$^-$/6W**), and (c) a four-carboxylate layer and a four-amide layer (Figure 3c,

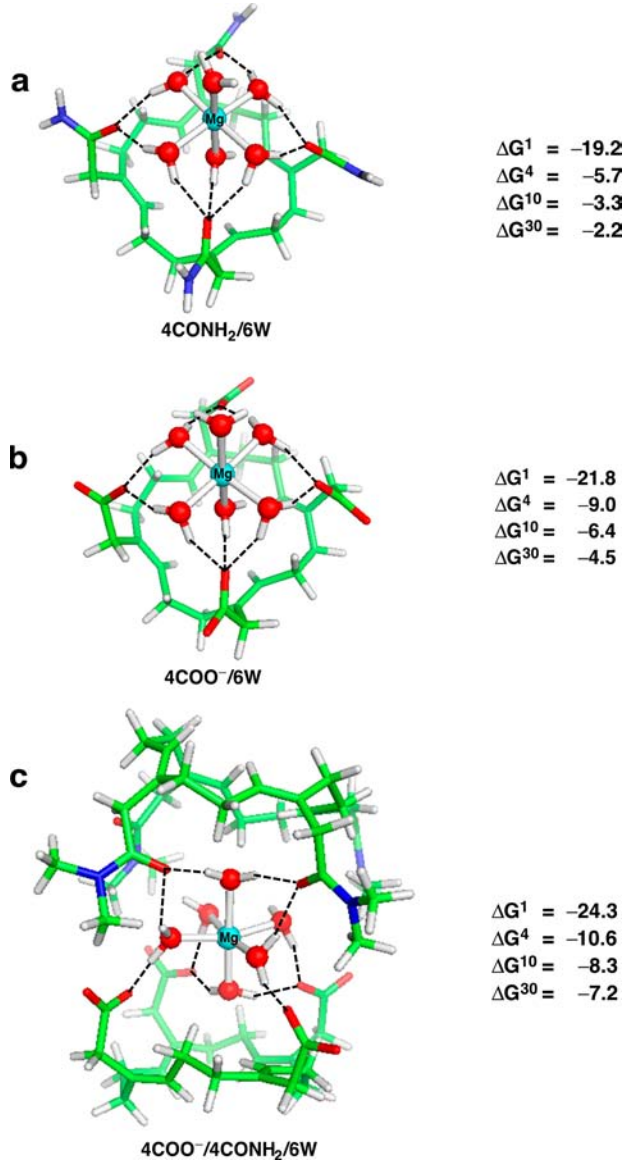

Figure 3. B3-LYP/6-31+G(3d,p) optimized structures of fully hexahydrated Mg^{2+} bound to tetrameric model selectivity filters comprising (a) four $CONH_2$ ligating groups, (b) four COO^- groups, and (c) four $CONH_2$ and four COO^- groups. The free energies ΔG^x (in kcal/mol) for replacing hexahydrated Ca^{2+} in the filter characterized by dielectric constant x with Mg^{2+} (eq 1) are shown on the right. The mean distances between Mg^{2+} and the four nearest carbonyl/carboxylate oxygen atoms in the **4CONH$_2$/6W**, **4COO$^-$/6W**, and **4COO$^-$/4CONH$_2$/6W** structures are 3.66, 3.49, and 3.70 Å, respectively.

dx.doi.org/10.1021/ja4087769 | J. Am. Chem. Soc. 2013, 135, 17200−17208

4COO⁻/4CONH₂/6W). In each model filter, the hexahydrated metal cation is stabilized by hydrogen bonds between its first-shell water molecules and surrounding carboxylate or carbonyl groups from the pore, as shown by the dashed lines in Figure 3. All these filters favor Mg^{2+} over Ca^{2+}, as evidenced by the favorable free energies for replacing $Ca^{2+}$with Mg^{2+} (negative ΔG^x). However, the Mg^{2+}/Ca^{2+} selectivity decreases with increasing dielectric constant x of the selectivity filter pore (ΔG^x becomes less negative with increasing x).

Selectivity for Mg^{2+} over Ca^{2+} is enhanced if the filter were lined with carboxylate rather than amide groups. The metal exchange free energies ΔG^x (x = 4–30) in the **4COO⁻/6W** filter are more favorable than those in the **4CONH₂/6W** filter by ~3 kcal/mol. This is apparently due to the protein environment rather than the metal-ligating groups lining the filter, because the gas-phase free energies for the **4CONH₂/6W** (−19.2 kcal/mol) and **4COO⁻/6W** (−21.8 kcal/mol) structures are very similar, despite significant differences in the electrostatic fields surrounding the passing hydrated ion in the **4CONH₂/6W** (0e) and **4COO⁻/6W** (−4e) filters. The similar ΔG^1 values imply that the interactions between the metal and its first hydration layer dominate the electrostatics of these complexes, while the amide/carboxylate groups from the second coordination shell have an auxiliary role. This is supported by the fact that the metal charges and the metal–O^{water} distances in the metal hydrates change negligibly upon coordination to the selectivity filter: The NBO charges on Mg^{2+} (1.76e) and Ca^{2+} (1.86e) in the free aqua complexes differ from those in the **4CONH₂/6W** and **4COO⁻/6W** filters by ≤0.02e, while the average Mg–O^{water} (2.10 Å) and Ca–O^{water} (2.42 Å) distances in the free metal hydrates differ from those in the two monolayered filters by ≤0.02 Å.

Adding another layer of "indirect" metal-ligating groups to a **4CONH₂/6W** or **4COO⁻/6W** filter helps to enhance the Mg^{2+}/Ca^{2+} selectivity. Relative to the single-layered **4CONH₂/6W** or **4COO⁻/6W** filters (Figure 3a,b), the two-layered filter (**4COO⁻/4CONH₂/6W**, Figure 3c) exhibits stronger preference for Mg^{2+}, as the Mg^{2+} aqua complex inside the bilayered filter cavity is better stabilized than the Ca^{2+} aqua complex: The gas-phase ΔG^1 free energy for replacing hexahydrated Ca^{2+} with hexahydrated Mg^{2+} in the two-layered filter is more favorable than that in the monolayered **4CONH₂/6W** or **4COO⁻/6W** filter by 5.1 and 2.5 kcal/mol, respectively. The protein environment does not change the observed gas-phase free energy trends.

Pentameric Filters. The selectivity filter of the homopentameric Mg^{2+}-selective CorA channel has an estimated pore diameter of ~8 Å,[18] which is just large enough to accommodate $Mg(H_2O)_6$ and $Ca(H_2O)_6$, whose diameters are found herein to be ~5.5 and ~6.1 Å, respectively. However, it is not clear whether the metal binds to the Gly/Asn amide groups from the conserved "GMN" motif[18] or to the Glu carboxylates from the "MPEL" motif[12,19,20] or to both. Hence, the putative selectivity filter(s) in the CorA Mg^{2+} channel have been modeled by pentameric selectivity filters lined with (a) a single layer of $CONH_2$ groups modeling the Gly/Asn amide groups from the "GMN" motif (Figure 4a; **5CONH₂/6W**), (b) a single layer of COO^- groups modeling the Glu carboxylates from the "MPEL" motif (Figure 4b; **5COO⁻/6W**), and (c) a five-carboxylate layer and a five-amide layer (Figure 4c; **5COO⁻/5CONH₂/6W**). Like their tetrameric analogues, these pentameric filters also favor Mg^{2+} over Ca^{2+} (negative ΔG^x; x = 4–30). Also in analogy to the tetrameric filters, selectivity for Mg^{2+} over Ca^{2+} is enhanced if (i) the pentameric filters were lined with carboxylate rather than amide groups (the ΔG^x values in Figure 4b are more negative than those in Figure 4a by 4 to 5 kcal/mol) or (ii) if it contained an additional layer of "indirect" metal-ligating groups (the ΔG^x values in Figure 4c are more negative than those in Figures 4a and 4b by ~7 and ~3 kcal/mol, respectively).

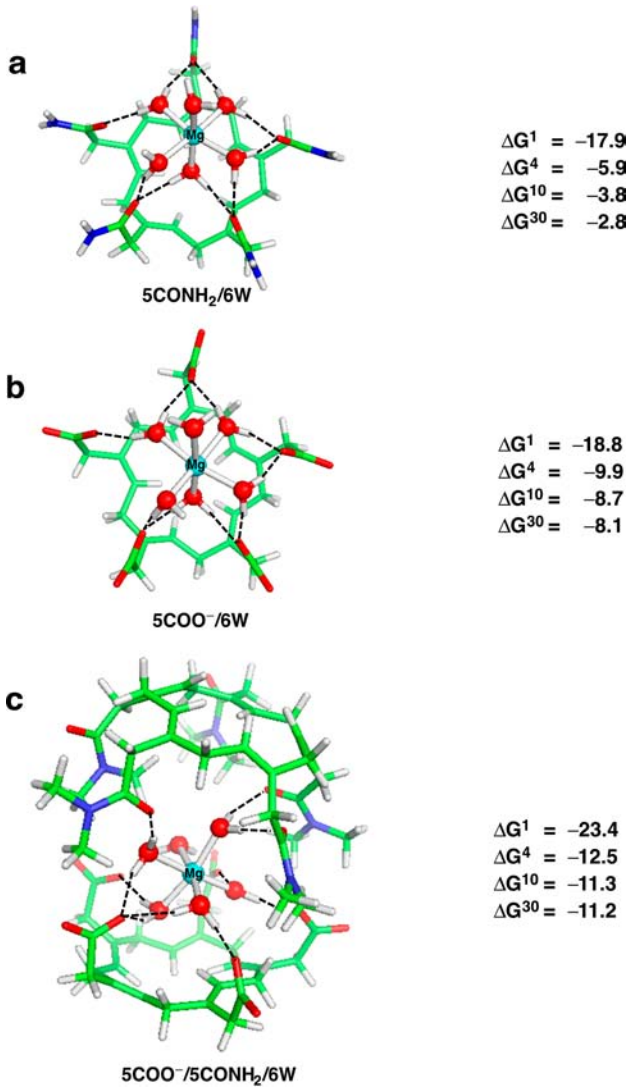

Figure 4. B3-LYP/6-31+G(3d,p) optimized structures of fully hexahydrated Mg^{2+} bound to pentameric model selectivity filters comprising (a) five $CONH_2$ ligating groups, (b) five COO^- groups, and (c) five $CONH_2$ and five COO^- groups. The free energies ΔG^x (in kcal/mol) for replacing hexahydrated Ca^{2+} in the filter characterized by dielectric constant x with hexahydrated Mg^{2+} (eq 1) are shown on the right. The mean distances between Mg^{2+} and the five nearest carbonyl/carboxylate oxygen atoms in the **5CONH₂/6W**, **5COO⁻/6W**, and **5COO⁻/5CONH₂/6W** structures are 3.93, 3.89, and 4.06 Å, respectively.

Comparison of the ΔG^x for the pentameric filters with the ΔG^x for the respective tetrameric filters shows that increasing the oligomericity does not significantly affect the Mg^{2+}/Ca^{2+} selectivity in monolayered filters lined with only amide groups: the ΔG^x (x = 4–30) values of tetrameric **4CONH₂/6W** and pentameric **5CONH₂/6W** filters differ by ≤0.6 kcal/mol. However, increasing the overall charge of the pore may slightly improve selectivity for Mg^{2+} over Ca^{2+} in filters characterized by

dx.doi.org/10.1021/ja4087769 | J. Am. Chem. Soc. 2013, 135, 17200–17208

an effective dielectric constant ≥30. The ΔG^{30} values of the pentameric **5COO$^-$/6W** and **5COO$^-$/5CONH$_2$/6W** filters with an overall charge of −5 are more favorable than those of the respective tetrameric filters with a net charge of −4 by ∼4 kcal/mol.

IV. DISCUSSION

Determinants of Mg^{2+}/Ca^{2+} Selectivity in Mg^{2+} Channel Selectivity Filters. The results herein indicate that the pore size and rigidity of the selectivity filter, which correlate with the degree of hydration of the permeable metal ion, is a key determinant of the Mg^{2+}/Ca^{2+} selectivity in Mg^{2+} channels. Wide pores that accommodate hexahydrated metal ions are Mg^{2+}-selective (Figures 3 and 4, negative ΔG^x). In such *wide* pores, the metal ions interact *indirectly* with the protein ligands via their first-shell water molecules, hence the metal desolvation and steric repulsion among the "indirect" metal-ligating groups become less important than the water-mediated interactions between the metal and the protein. As Mg^{2+}, being a stronger electron acceptor, polarizes the bound water molecules more than Ca^{2+} or monocations, the Mg^{2+}—water—protein interactions are stronger than the corresponding interactions with hexahydrated Ca^{2+}, Na^+, or K^+, thus favoring hexahydrated Mg^{2+} in a wide pore. On the other hand, narrow pores that fit dehydrated metal ions are Ca^{2+}-selective (Figure 1, positive ΔG^x). In such *narrow* pores, the metal ions interact *directly* with the carbonyl/carboxylate groups lining the filter, hence metal desolvation becomes critical unlike in the wide pores that do not require the metal cations to be dehydrated. As Ca^{2+} has a smaller dehydration penalty than Mg^{2+}, it is favored over Mg^{2+} in a narrow pore. The different pore size requirements of Mg^{2+} and Ca^{2+} implies that the selectivity filter should be rigid enough to maintain the optimal pore size and the corresponding degree of metal hydration of the cognate metal cation. It would be interesting to confirm these findings by all-atom molecular dynamics free energy simulations[45,46] (which account explicitly for the influence of flexibility and protein dynamics on ion selectivity) using force fields including charge transfer and polarization effects[47,48] when high-resolution structures of the native metal ion bound in Mg^{2+} and Ca^{2+} channels become available.

Compared to the pore size/rigidity of the selectivity filter, the net charge of the metal-ligating residues lining the Mg^{2+} channel selectivity filter act as a second-order selectivity determinant, as it affects the Mg^{2+}/Ca^{2+} selectivity to a lesser extent. Pentameric filters lined with carboxylates exhibit a stronger preference for Mg^{2+} than those lined with amides: relative to the ΔG^x for the **5CONH$_2$/6W** filter, the ΔG^x for the **5COO$^-$/6W** and **5COO$^-$/5CONH$_2$/6W** filters are more negative by 4−5 and 7−8 kcal/mol, respectively. On the other hand, the solvent accessibility and the oligomeric state of the channel do not seem to significantly affect the Mg^{2+}/Ca^{2+} selectivity. Pores that allow for hexahydrated ions to pass are Mg^{2+}-selective, regardless of their solvent exposure (Figures 3 and 4, negative ΔG^x for x = 4−30). Tetrameric **4CONH$_2$/6W** and pentameric **5CONH$_2$/6W** filters exhibit nearly identical Mg^{2+}/Ca^{2+} selectivity (ΔG^x in Figures 3a and 4a differ by <1 kcal/mol). This is in accord with the fact that homotetrameric TRPM6[13] and homopentameric CorA[17,18] are both Mg^{2+}-selective. Although tetrameric and pentameric filters with pores that can accommodate hexahydrated metal ions can both select Mg^{2+} over Ca^{2+}, a bilayered pentameric **5COO$^-$/5CONH$_2$/6W** seems to best discriminate the "native" Mg^{2+} from its key rival, Ca^{2+}.

Comparison of the Ion Selectivity Determinants in Various Channels. The selectivity filter in the Mg^{2+} channel seems to play a primarily structural rather than a physicochemical role by maintaining a wide enough pore to accommodate hexahydrated cations that interact indirectly with the ligands lining the pore. In contrast, the selectivity filters in K^+, Na^+, and Ca^{2+} channels have narrower pores so their ligands interact directly with a dehydrated or partially hydrated cation. Hence, in addition to the size and rigidity of the pore, the composition (number and charge/charge-donating ability of metal-ligating residues) and the solvent accessibility of the selectivity filter dictate the outcome of the competition between the native metal ion and its key rival cation in K^+, Na^+, and Ca^{2+} channels, as outlined below.

In the homotetrameric KcsA K^+ channels, the selectivity filter provides eight weak-ligating backbone carbonyl oxygen atoms lining a relatively rigid, solvent-inaccessible pore that favors an octahydrated K^+.[26,49] Such a filter selects K^+ over Na^+ because (i) the rigidity of the pore forces the competing Na^+ to adopt the 8-fold coordination for K^+ and prohibits Na^+ from adopting its preferred coordination geometry, (ii) the weak ligating strength of the carbonyl ligands cannot offset the larger cost of dehydrating Na^+, as compared to K^+, and (iii) more water molecules are released upon binding octahydrated K^+ than hexahydrated Na^+ in the selectivity filter of K^+ channel.[26,49−53]

In vertebrate Na_v channels, the DEKA filter provides three rather than four ligands as the Lys does not bind the metal cation but rigidifies and constricts the pore by forming hydrogen bonds with the neighboring Asp/Glu carboxylate and Ala backbone carbonyl oxygen atoms.[27] Such a filter selects Na^+ over K^+ because (i) the narrow and rigid pore fits Na^+ nicely, but not the larger K^+, and (ii) the strong ligating strength of the Asp/Glu carboxylates helps to offset the larger dehydration penalty of Na^+ compared to that of K^+.[27] Whereas the aperture of the DEKA filter is small and fits dehydrated Na^+, that of the EEEE filter in bacterial Na_v channels is much wider, compatible with partially hydrated Na^+ binding indirectly to two or more Glu carboxylates.[28,54] Such a EEEE filter favors Na^+ over K^+ because the bulkier hydrated K^+ cannot fit in-plane with water molecules bridging to the carboxylates and thus binds less favorably than Na^+ to the four glutamates.[55]

Interestingly, high voltage-activated Ca_v channels also possess EEEE filters but they are highly selective for Ca^{2+} over Na^+. Unlike the bacterial Na_v channels, the pores of high voltage-activated Ca_v channels are more constricted with an estimated aperture area of 18.0−19 Å^2 that is compatible with monohydrated Ca^{2+}.[56] Such a filter selects Ca^{2+} over Na^+ because compared to monocationic Na^+ (i) electrostatic interactions of the four Glu carboxylates with dicationic Ca^{2+} are more favorable, overcoming the greater dehydration penalty of Ca^{2+},[28,30,57−59] and (ii) more water molecules are freed when Ca^{2+} is bound to the selectivity filter.[30]

Biological Implications. Our results are consistent with experimental data (see below) and help to explain some experimental findings. They confirm the hypothesis put forth by Moomaw and Maguire[20] that the CorA Mg^{2+} ion channel recognizes specifically hexahydrated Mg^{2+}, as opposed to dehydrated or partially hydrated Mg^{2+} (see Figure 2).[18,20] They also predict that the TRPM6 channel, like the CorA Mg^{2+} ion channel, is also specific for hexahydrated Mg^{2+} (negative ΔG^x in Figure 3). Thus, a key unifying feature of the Mg^{2+}

dx.doi.org/10.1021/ja4087769 | J. Am. Chem. Soc. 2013, 135, 17200−17208

channel selectivity filters that accounts for their Mg^{2+} selectivity is a sufficiently wide and relatively rigid pore that allows hexahydrated Mg^{2+} to pass through. This feature of the selectivity filter makes Mg^{2+} ion channels unique among the family of cation-selective ion channels.

Homotetrameric TRPM6 Ion Channel. The carboxylate-containing monolayer filter, **4COO$^-$/6W**, is more selective for Mg^{2+} than its amide counterpart **4CONH$_2$/6W** (ΔG^x in Figure 3b is more negative than those in Figure 3a). This finding is in accord with experimental findings that D1031 is conserved throughout the entire TRPM subfamily and its mutation to alanine abolished the channel's function, whereas I1030 is less conserved and its mutation to methionine retained the channel's function.[14] Adding another layer of "indirect" metal-ligating amide groups to a large **4COO$^-$/6W** filter may slightly improve the Mg^{2+}/Ca^{2+} selectivity, as the metal exchange free energies in the **4COO$^-$/4CONH$_2$/6W** (Figure 3c) are more favorable than those in the **4COO$^-$/6W** (Figure 3b). Thus, a bilayer selectivity filter in TRPM6 consisting of a ring of four D1031 carboxylates and a ring of four I1030 amide groups would be expected to be the most selective for Mg^{2+} over Ca^{2+}.

Homopentameric CorA Ion Channel. Both mono- and bilayered pentameric selectivity filters that can accommodate hexahydrated Mg^{2+} are highly Mg^{2+}-selective (Figure 4, negative ΔG^x). These findings are consistent with the two types of selectivity filters proposed for the CorA Mg^{2+} channels, namely, the EEEEE locus from the "MPEL" motif in *St*CorA[12,19,20] (corresponding to **5COO$^-$/6W**, Figure 4b) or the NNNNN locus from the nearby "GMN" motif[16−18,60,61] (corresponding to **5CONH$_2$/6W**, Figure 4a). Furthermore, the fully optimized structures of the model pentameric filters shown in Figure 4 are consistent with the CorA crystal structures. The mean distance between Mg^{2+} and the five carbonyl oxygen atoms in the **5CONH$_2$/6W** structure (3.93 Å) agrees with that between Mg^{2+} and the five carbonyl oxygen atoms of Gly312 from the "GMN" motif in the 2.7 Å crystal structure of *Tm*CorA (3.97 Å, PDB code 4i0u). The pore aperture area, estimated by the area of the pentagon formed by the five carbonyl oxygen atoms in the **5CONH$_2$/6W** structure (32 Å^2) also agrees with that in the *Tm*CorA crystal structure (35 Å^2). The **5COO$^-$/6W** filter (Figure 4b) is predicted to be more selective than the corresponding **5CONH$_2$/6W** one (Figure 4a). However, in the 2.7 Å *Tm*CorA structure (PDB code 4i0u), no metal ion was detected near the "MPEL" segment of the periplasmic loop where the Glu side chain was found to face away from the pore lumen.[17] Furthermore, the periplasmic loops of a few CorA channels such as *Mj*CorA do not contain the "MPEL" motif but are still Mg^{2+}-selective.[20] Thus, it appears that some CorA channels may employ a less Mg^{2+}/Ca^{2+} -selective pentameric filter lined with amide groups from the "GMN" motif (**5CONH$_2$/6W**, Figure 4a) instead of Glu carboxylates from the "MPEL" motif.

AUTHOR INFORMATION

Corresponding Author

carmay@gate.sinica.edu.tw; t.dudev@chem.uni-sofia.bg

Present Address

[§]T.D.: Faculty of Chemistry and Pharmacy, Sofia University, Sofia 1164, Bulgaria.

Notes

The authors declare no competing financial interest.

ACKNOWLEDGMENTS

This work is supported by Academia Sinica and the NSC (Contract No. 95-2113-M-001-001). T.D. is supported by the Institute of Biomedical Sciences at Academia Sinica and EU grant "Beyond Everest" FP7-REGPOT-2011-1.

REFERENCES

(1) Maguire, M. E.; Cowan, J. A. *Biometals* **2002**, *15*, 203.
(2) Romani, A.; Scarpa, A. *Arch. Biochem. Biophys.* **1992**, *298*, 1.
(3) Scarpa, A.; Brinley, F. J. *Fed. Proc.* **1981**, *40*, 2646.
(4) Dalmas, O. *Biophys. J.* **2007**, *93*, 3729.
(5) Romani, A. M. P. *Arch. Biochem. Biophys.* **2011**, *512*, 1.
(6) Cowan, J. A. *Biological Chemistry of Magnesium*; VCH: New York, 1995.
(7) Garcia-Vescovi, E.; Soncini, F. C.; Groisman, E. A. *Cell* **1996**, *84*, 165.
(8) Dudev, T.; Cowan, J. A.; Lim, C. *J. Am. Chem. Soc.* **1999**, *121*, 7665.
(9) Dudev, T.; Lim, C. *J. Phys. Chem. A* **1999**, *103*, 8093.
(10) Alexander, R. T.; Hoenderop, J. G.; Bindels, R. J. *J. Am. Soc. Nephrol.* **2008**, *19*, 1452.
(11) Maguire, M. E. *Front. Biosci.* **2006**, *11*, 3149.
(12) Moomaw, A. S.; Maguire, M. E. *Physiology* **2008**, *23*, 275.
(13) Voets, T.; Nilius, B.; van der Kemp, A. W.; Droogmans, G.; Bindels, R. J.; Hoenderop, J. G. *J. Biol. Chem.* **2004**, *279*, 19.
(14) Topala, C. N.; Groenestege, W. T.; Thebault, S.; van den Berg, D.; Nilius, B.; Hoenderop, J. G.; Bindels, R. J. *Cell Calcium* **2007**, *41*, 513.
(15) Lunin, V. V.; Dobrovetsky, E.; Khutoreskaya, G.; Zhang, R.; Joachimiak, A.; Doyle, D. A.; Bochkarev, A.; Maguire, M. E.; Edwards, A. M.; Koth, C. M. *Nature* **2006**, *440*, 833.
(16) Payandeh, J.; Pai, E. F. *EMBO J.* **2006**, *25*, 3762.
(17) Nordin, N.; Guskov, A.; Phua, T.; Sahaf, N.; Xia, Y.; Siyan, L.; Eshaghi, H.; Eshaghi, S. *Biochem. J.* **2013**, *451*, 365.
(18) Guskov, A.; Nordin, N.; Reynaud, A.; Engman, H.; Lundback, A.-K.; Kong, A. J. O.; Cornvik, T.; Phua, T.; Eshaghi, S. *Proc. Natl. Acad. Sci. U.S.A.* **2012**, *109*, 18459.
(19) Maguire, M. E. *Curr. Opin. Struct. Biol.* **2006**, *16*, 432.
(20) Moomaw, A. S.; Maguire, M. E. *Biochemistry* **2010**, *49*, 5998.
(21) Dudev, T.; Lim, C. *J. Phys. Chem. B* **2001**, *105*, 4446.
(22) Babu, C. S.; Dudev, T.; Casareno, R.; Cowan, J. A.; Lim, C. *J. Am. Chem. Soc.* **2003**, *125*, 9318.
(23) Dudev, T.; Lim, C. *J. Phys. Chem. B* **2004**, *108*, 4546.
(24) Dudev, T.; Chang, L.-Y.; Lim, C. *J. Am. Chem. Soc.* **2005**, *127*, 4091.
(25) Dudev, T.; Lim, C. *J. Am. Chem. Soc.* **2011**, *133*, 9506.
(26) Dudev, T.; Lim, C. *J. Am. Chem. Soc.* **2009**, *131*, 8092.
(27) Dudev, T.; Lim, C. *J. Am. Chem. Soc.* **2010**, *132*, 2321.
(28) Dudev, T.; Lim, C. *Phys. Chem. Chem. Phys.* **2012**, *14*, 12451.
(29) *GaussView*, version 3.09; Gaussian: Pittsburgh, PA, 2000−2003.
(30) Dudev, T.; Lim, C. *J. Phys. Chem. B* **2012**, *116*, 10703.
(31) Marcus, Y. *Chem. Rev.* **1988**, *88*, 1475.
(32) Dudev, M.; Wang, J.; Dudev, T.; Lim, C. *J. Phys. Chem. B* **2006**, *110*, 1889.
(33) Frisch, M. J.; Trucks, G. W.; Schlegel, H. B.; Scuseria, G. E.; Robb, M. A.; Cheeseman, J. R.; Scalmani, G.; Barone, V.; Mennucci, B.; Petersson, G. A.; Nakatsuji, H.; Caricato, M.; Li, X.; Hratchian, H. P.; Izmaylov, A. F.; Bloino, J.; Zheng, G.; Sonnenberg, J. L.; Hada, M.; Ehara, M.; Toyota, K.; Fukuda, R.; Hasegawa, J.; Ishida, M.; Nakajima, T.; Honda, Y.; Kitao, O.; Nakai, H.; Vreven, T.; Montgomery, J. A., Jr.; Peralta, J. E.; Ogliaro, F.; Bearpark, M.; Heyd, J. J.; Brothers, E.; Kudin, K. N.; Staroverov, V. N.; Kobayashi, R.; Normand, J.; Raghavachari, K.; Rendell, A.; Burant, J. C.; Iyengar, S. S.; Tomasi, J.; Cossi, M.; Rega, N.; Millam, J. M.; Klene, M.; Knox, J. E.; Cross, J. B.; Bakken, V.; Adamo, C.; Jaramillo, J.; Gomperts, R.; Stratmann, R. E.; Yazyev, O.; Austin, A. J.; Cammi, R.; Pomelli, C.; Ochterski, J. W.; Martin, R. L.; Morokuma, K.; Zakrzewski, V. G.; Voth, G. A.; Salvador, P.; Dannenberg, J. J.; Dapprich, S.; Daniels, A. D.; Farkas, O.;

Foresman, J. B.; Ortiz, J. V.; Cioslowski, J.; Fox, D. J. *Gaussian 09*; Gaussian, Inc.: Wallingford CT, 2009.
(34) Wong, M. W. *Chem. Phys. Lett.* **1996**, *256*, 391.
(35) Gilson, M., K.; Honig, B., H. *J. Comput. Chem.* **1988**, *9*, 327.
(36) Lim, C.; Bashford, D.; Karplus, M. *J. Phys. Chem.* **1991**, *95*, 5610.
(37) Bashford, D. In *Scientific Computing in Object-Oriented Parallel Environments*; Ishikawa, Y., Oldehoeft, R. R., Reynders, V. W., Tholburn, M., Eds.; Springer: Berlin, 1997; Vol. *1343*, p 233.
(38) Dudev, T.; Lim, C. *J. Am. Chem. Soc.* **2006**, *128*, 1553.
(39) Reed, A.; Weinstock, R.; Weinhold, F. *J. Chem. Phys.* **1985**, *83*, 735.
(40) Brooks, B. R.; Bruccoleri, R. E.; Olafson, B. D.; aStates, D. J.; Swaminathan, S.; Karplus, M. *J. Comput. Chem.* **1983**, *4*, 187.
(41) Dudev, T.; Lim, C. *J. Am. Chem. Soc.* **2009**, *131*, 8092.
(42) Ozutsumi, K.; Ishigiro, S. *Bull. Chem. Soc. Jpn.* **1992**, *65*, 1173.
(43) Smith, R. M.; Martell, A. E. *Sci. Total Environ.* **1987**, *64*, 125.
(44) Dudev, T.; Lim, C. *Phys. Chem. Chem. Phys.* **2012**, *14*, 12451.
(45) Luzhkov, V. B.; Aqvist, J. *Biochim, Biophys. Acta* **2001**, *1548*, 194.
(46) Noskov, S. Y.; Roux, B. *J. Gen. Physiol.* **2007**, *129*, 135.
(47) Sakharov, D.; Lim, C. *J. Am. Chem. Soc.* **2005**, *127*, 4923.
(48) Babu, C. S.; Lim, C. *J. Phys. Chem. A* **2006**, *110*, 691.
(49) Varma, S.; Rempe, S. B. *Biophys. J.* **2007**, *93*, 1093.
(50) Zhou, Y.; Morais-Cabral, J. H.; Kaufman, A.; MacKinnon, R. *Nature* **2001**, *414*, 43.
(51) Bostick, D. L.; Brooks, C. L., III *Proc. Natl. Acad. Sci. U.S.A.* **2007**, *104*, 9260.
(52) Varma, S.; Sabo, D.; Rempe, S. B. *J. Mol. Biol.* **2008**, *376*, 13.
(53) Fowler, P. W.; Tai, K.; Sansom, M. S. P. *Biophys. J.* **2008**, *95*, 5062.
(54) Payandeh, J.; Scheuer, T.; Zheng, N.; Catterall, W. A. *Nature* **2011**, *475*, 353.
(55) Corry, B.; Thomas, M. *J. Am. Chem. Soc.* **2012**, *134*, 1840.
(56) McCleskey, E. W.; Almers, W. *Proc. Natl. Acad. Sci. U.S.A.* **1985**, *82*, 7149.
(57) Boda, D.; Valisko, M.; Henderson, D.; Eisenberg, B.; Gillespie, D.; Nonner, W. *J. Gen. Physiol.* **2009**, *133*, 497.
(58) Eisenberg, B. *Biophys. Chem.* **2003**, *100*, 507.
(59) Nonner, W.; Catacuzzeno, L.; Eisenberg, B. *Biophys. J.* **2000**, *79*, 1976.
(60) Eshaghi, S.; Niegowski, D.; Kohl, A.; Molina, D. M.; Lesley, S. A.; Nordlund, P. *Science* **2006**, *313*, 354.
(61) Pfoh, R.; Li, A.; Chakrabarti, N.; Payandeh, J.; Pomes, R.; Pai, E. F. *Proc. Natl. Acad. Sci. U.S.A.* **2012**, *109*, 18809.